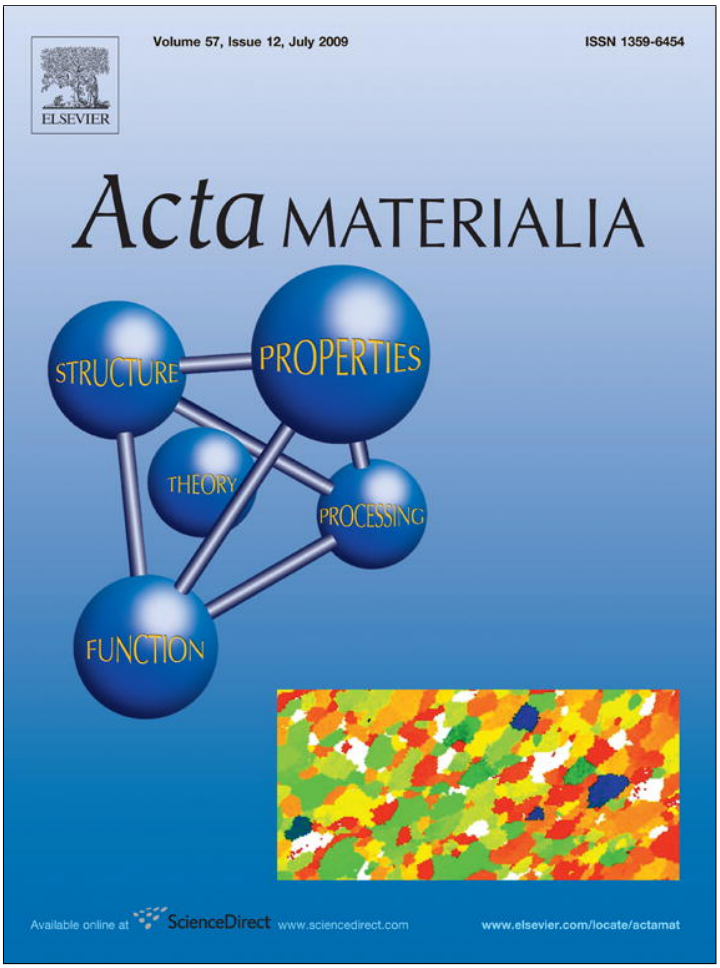

Available online at www.sciencedirect.com
ScienceDirect
Acta Materialia 57 (2009) 3662–3670
Acta MATERIALIA
www.elsevier.com/locate/actamat

Anomalous triple junction surface pits in nanocrystalline zirconia thin films and their relationship to triple junction energy

Hakkwan Kim [a,1], Yi Xuan [b], Peide D. Ye [b], Raghavan Narayanan [a,2], Alexander H. King [a,*]

[a] School of Materials Engineering, Purdue University, West Lafayette, IN 47907, USA
[b] Birck Nanotechnology Center and School of Electrical and Computer Engineering, Purdue University, West Lafayette, IN 47907, USA

Received 9 January 2009; received in revised form 19 April 2009; accepted 21 April 2009
Available online 19 May 2009

Abstract

Triple junctions (TJs) are the lines where three grains or grain boundaries meet and become increasingly important in nanocrystalline materials where they have a high areal number density and occupy a significant fraction of the total volume of the material. Surface pits are associated with TJs, just as surface grooves are associated with grain boundaries, and these pits may have particularly deleterious effects on the behaviors of thin films. We evaluate the surface topography associated with TJs in nanocrystalline ZrO_2 thin films using thickness mapping images produced by energy-filtered transmission electron microscopy (EFTEM), and compare our results with theoretical predictions. While many of the pits conform to the standard theoretical treatment, some of them exhibit considerably increased depth, possibly indicating that the junctions have line energy. No pits were observed with less than the theoretically predicted depth.

Keywords: Transmission electron microscopy (TEM); Crystalline oxides; Thin films; Surface structure; Interface defects

1. Introduction

Triple junctions (TJs) are the lines where three grain boundaries meet, and interest in their behavior has been growing in recent years, since they may exert a considerable influence on polycrystalline materials, especially in the nanocrystalline regime. TJs are line defects that can significantly influence the mechanical, thermodynamic and kinetic properties of polycrystalline materials. Previous studies have shown that TJs are preferential sites for chemical attack [1], they are implicated in the formation of electromigration damage in thin conductor lines [2], and chemical segregation to TJs can exceed the segregation at grain boundaries by a large factor [3]. They also appear to affect the kinetics of grain growth in certain circumstances [4]. Because the grain morphology in polycrystalline thin films can affect the continuity, reactivity and strength of the film, TJs may impact these properties if they affect the surface morphology [5]. It is therefore of great importance to know how TJ properties vary in order to predict the behavior of polycrystalline thin films and bulk materials. Zirconia, in particular, has potential applications in solid oxide fuel cells, and it is essential for this application that the material should have no pinholes, which might be associated with TJs.

Experimental measurements of basic TJ properties such as their energy are still elusive. It is even unknown whether TJs have energies that are greater or smaller than the grain boundaries that they adjoin. Since McLean [6] first proposed that TJ energy should be positive because atoms at these sites would be under the influence of three rather than two competing forces, several experiments and simulation studies confirmed his suggestion [7,8]. Fortier et al. [9] were the first to use the direct measurement of surface topogra-

* Corresponding author. Present address: The Ames Laboratory, Ames, IA 50011, USA. Tel.: +1 515 294 2770; fax: +1 515 294 4456.
E-mail address: alexking@ameslab.gov (A.H. King).
[1] Electro Materials and Device Lab., Samsung Electro-Mechanics Co., Ltd. 314, Maetan3-Dong, Yeongtong-Gu, Suwon, Gyunggi-Do 443-743, South Korea.
[2] Intel Corporation, Chandler, AZ 85226, USA.

1359-6454/$36.00
doi:10.1016/j.actamat.2009.04.032

phy to show that certain TJs can display behavior consistent with a significant positive excess free energy, in high-purity copper sheets.

Other researchers, however, suggest that TJs can have a negative energy per unit length. Gibbs [10] discussed the possibility that the excess free energy of a TJ among fluid phases, which he termed line tension, could be negative, and Srinivasan et al. [11] also demonstrated, using computer simulation, that the excess energies of grain boundary TJs might be negative.

King [12] has considered the complications of making unambiguous measurements of TJ energy, either in computer simulations or laboratory experiments. He concluded that experimental measurements of TJ energy have not yet produced any unambiguously reliable results, although a number of attempts have been made.

The aim of this work is to apply a simple experimental method to evaluate TJ-related surface topography in nanocrystalline thin films of single-phase cubic zirconia, to identify whether or not the depths of surface pits at the TJs can be predicted reliably from standard theoretical approaches. As suggested by Fortier et al. [9], increased pit depth at a TJ may be associated with a positive TJ energy, and decreased depth may indicate a negative TJ energy, so our results may be interpreted in terms of the existence of non-zero TJ energy or line tension.

2. Materials and methods

Fully dense polycrystalline pure ZrO_2 thin films with a nominal thickness of 20 nm were grown at a substrate temperature of 300 °C by the atomic layer deposition (ALD) method, using an ASM Microchemistry F-120 ALCVD™ reactor, onto amorphous, 30 nm thick Si_3N_4 membrane window substrates supported by single-crystal Si wafers. The films were annealed at $0.4T_m$ (922 °C) for 1 h to obtain a columnar microstructure with grain boundaries aligned perpendicular to the film surface. Carbon was sputtered onto the specimens used for transmission electron microscopy (TEM), to prevent charge build-up which can cause the specimen to drift and crack under the electron beam.

Thickness mapping images in the annealed films were obtained by field emission TEM using a FEI Titan 80/300 microscope equipped with a Gatan imaging filter (GIF) and operated at a voltage of 300 kV. The images were recorded with a slow scan CCD camera within the GIF and all electron energy loss spectra and energy-filtering TEM (EFTEM) images/maps were acquired using the Gatan® Digital Micrograph® software, version 3.65. The image acquisition time was 20 s. Although it was possible to gather more signal if we increased the acquisition times, we limited the times to 20 s to prevent the problem of specimen drift between the successive images needed for a thickness map, and also to limit radiation damage. The width of the energy-selecting slit was chosen to optimize the signal-to-noise ratio. Thickness maps were obtained using the log-ratio method [13], which is the most widely used procedure for measuring specimen thickness within a region defined by the incident beam. The software automatically integrates and compares the area I_0 under the zero-loss peak with the total area I_t under the whole electron energy loss spectrum. Therefore, we can obtain final thickness maps after acquiring zero-loss and plasmon images successively. The log-ratio formula [14] is then computed, providing relative thickness maps. These maps contain information about the relative film thickness for each pixel, and line scans across these images show thickness gradients. Line profiles giving the film thicknesses along grain boundaries were acquired from the mapping image files using the public-domain software Image J [15].

3. Geometrical approach

In order to assess whether the intersection of a TJ with a free surface is at, above or below its expected depth, we must first establish a means of identifying the expected depth.

Nishimura [16] first suggested a geometrical analysis for the thermal etching characteristics of TJs. On the basis of this study, Fortier et al. [9] estimated TJ energy by observing grain boundary groove depths in the vicinity of a TJ-free surface intersection using scanning tunneling microscopy (STM). Their assumptions were: (i) grain boundaries intersect at 120°; (ii) interfacial torque is zero; (iii) TJ excess energy is a constant; and (iv) the grain boundary groove angles and groove depths are constant. They represented the local geometry at thermally etched junctions as piecewise planar surfaces, represented by irregular tetrahedra, and showed that the geometric characteristics of these tetrahedra could be a function of (i) grain boundary groove angles and depths, (ii) free surface energies and (iii) TJ energies. For a system with grain boundary to surface energy ratio 0.3, they concluded that the groove depth at a TJ should be 33% deeper than the adjoining grain boundary groove in the absence of any excess TJ energy.

For our purposes, a slightly more detailed analysis is required. We first consider an idealized surface intersected by a regular hexagonal network of grain boundaries, as shown in Fig. 1. If all of the surface energies and grain boundary energies are uniform and isotropic, and the TJ energies are negligible, then after equilibration the surface of each grain is a spherical cap, and the intersection of each grain boundary plane with the surface will describe a circular arc in a vertical plane. The entire surface can be represented by three characteristic measurements of the surface height: z_c, the height at the center of a grain, z_{gb}, the height at the center of a grain boundary segment, and z_{tj}, the height at a TJ. The depth of the cusp at a TJ can then be represented dimensionlessly as the "reduced depth" [5]:

$$H_r = \frac{z_c - z_{tj}}{z_c - z_{gb}} \tag{1}$$

The surface groove angles for the grain boundaries are determined by the ratio of the grain boundary and surface

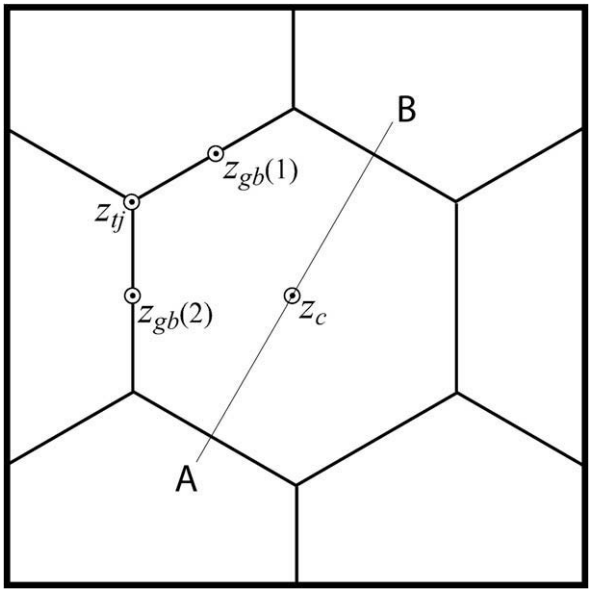

Fig. 1. Schematic plan view of the surface of an idealized polycrystal with made up of uniform hexagonal grains. The locations of critical height measurements for Eq. (1) are indicated, and it is clear that the value of H_r is the same whether we use $Z_{gb}(1)$ or $Z_{gb}(2)$.

energies, via the Herring equation [17], and we find that the reduced depth is independent of the grain size. In the absence of anisotropy or TJ line tension, this depth is related to the grain boundary and surface energies by

$$H_r = \left\{1 - \sqrt{\frac{4}{3}\left[1 - \left(\frac{\gamma_g}{2\gamma_s}\right)^2\right] - \frac{1}{3}}\right\} \Big/ \left\{1 - \sqrt{\left[1 - \left(\frac{\gamma_g}{2\gamma_s}\right)^2\right]}\right\} \tag{2}$$

As seen in Fig. 2, this measure is almost constant for small values of γ_g/γ_s, rising slowly at first, from a limiting value of $H_r = 4/3$ (as soon as $\gamma_g/\gamma_s > 1$), to $H_r = 1.337$ at $\gamma_g/\gamma_s = 0.3$, which is the case considered by Nishimura [16]. We also find when γ_g/γ_s rises to the critical value of $\sqrt{3}$, H_r becomes infinite, corresponding to the formation of hollow TJs, or pinholes, even in the absence of any excess TJ energy. This condition occurs when the grain boundary groove root angle is 60° or smaller, so the polycrystal remains contiguous, despite having percolative open channels in place of solid TJs. The range of energy ratios presented here is rather extreme. For most metals and ceramics γ_g/γ_s falls in the range of 0.2–0.4, for which the TJ depth is almost constant.

In principle, we should be able to perform an experiment in which we measure γ_g/γ_s by determining the grain boundary groove root angle far away from a TJ, and use this to calculate the expected TJ cusp depth in terms of H_r. Larger than expected values of H_r would then correspond to positive TJ energies, just as suggested by Fortier et al. [9], but we have now dispensed with any assumptions concerning the ratio of γ_s to γ_g. There remain two flaws in this approach, however.

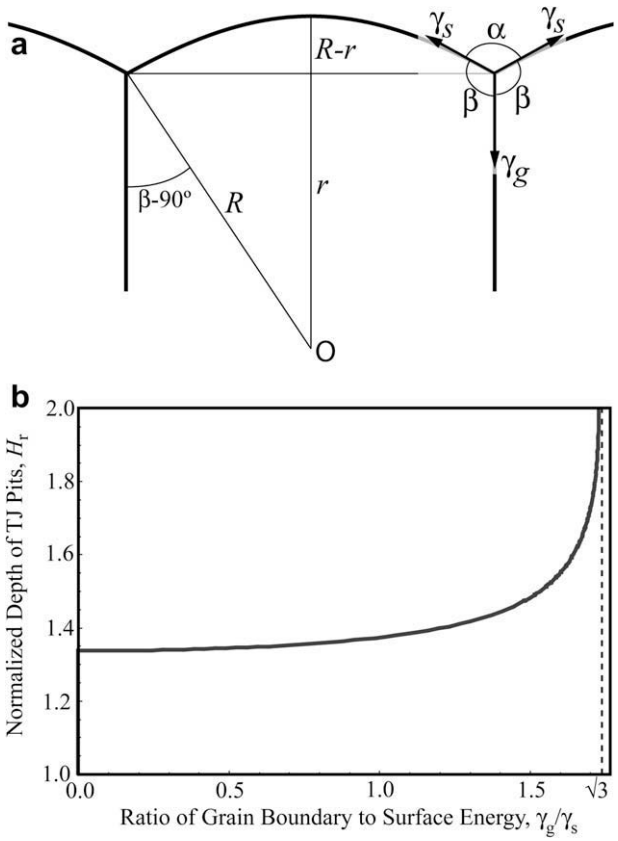

Fig. 2. (a) Cross-section on the vertical plane AB, indicated in Fig. 1, showing the essential geometry for calculating the normalized pit depth. (b) The normalized pit depth as a function of the ratio of grain boundary energy to surface energy. The pit depth becomes infinite, corresponding to hollow TJs, when $\gamma_g/\gamma_s = \sqrt{3}$, if the TJs embody no energy.

First, the analysis has been based on the assumption that there is no energy associated with the other TJs in the system, defined by the intersections of the grain boundaries with the surface. King [12] has pointed out that the raising or lowering of the grain boundary TJ cusp depends on the relative energies of the grain boundary TJ and the crystal–crystal–vapor TJs.

Second, the analysis also rests upon the assumption of a uniform hexagonal grain structure. When we consider a more realistic grain structure, with a distribution of grain sizes and edge lengths, the cusp geometry and the set of expected cusp depths also develops a significant distribution of values, as illustrated schematically in Fig. 3. H_r values measured using short grain boundary segments to provide the value of z_{gb} are inevitably different from the values measured using long grain boundary segments, and the distribution of the values, compounded with experimental error in their measurement, is likely to mask any actual change in the depth of a TJ cusp from its expected value [18].

We therefore adopt a modification of the approach first suggested by Fortier et al. [9], in which we evaluate the shapes of grain boundary surface grooves, along their entire length. As described above, in the absence of any

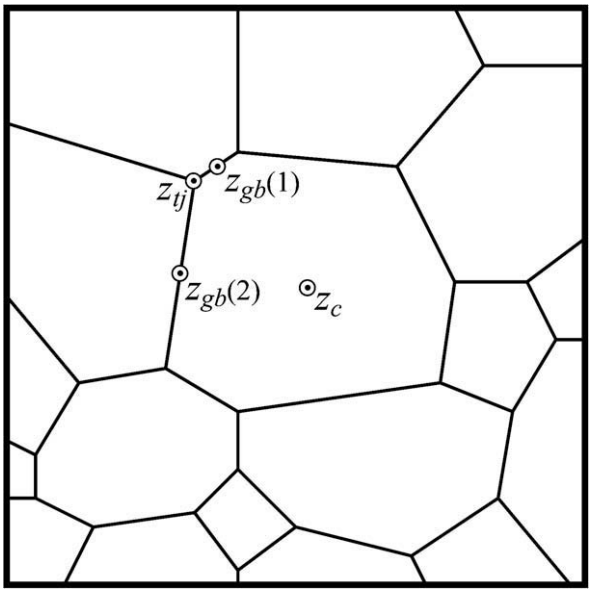

Fig. 3. Illustrating the problem of defining the normalized pit depth in a less-regular grain structure. The values of H_r are different if we use the two different values of Z_{gb}.

energy associated with the grain boundary TJs, the groove root should describe an arc of a circle. If there is a positive energy associated with the groove root itself (since it is a crystal–crystal–vapor TJ), then it will trace a curve of larger radius, but will still be a circular arc. Deviation from a circular path in a plane perpendicular to the film surface, particularly those deviations that occur at the ends of grain boundary segments, are expected to occur if the grain boundary TJs have line tensions.

4. Results

Fig. 4 shows plan-view images and one corresponding diffraction pattern representative of the materials used in this research. Fig. 4a is a bright-field image of vapor-deposited and annealed ZrO_2 film obtained at a magnification of 225,000×. Images of this kind from several different regions within the film show the average grain size to be 20 nm, which is approximately equal to the average film thickness, consistent with the usual sheet-thickness effect [19,20]. Fig. 4b is a high-resolution image of a TJ and its four adjoining grains. These images show that our thin films are columnar-grained and have the cubic crystal structure, which is frequently found to be stable in fine-grained pure zirconia thin films. The grain boundaries and TJs are not decorated with any obvious amorphous layers or second phases.

Fig. 5 shows a typical set of EFTEM images including multibeam, zero electron energy loss, plasmon loss and the corresponding thickness mapping image, in which the intensity is proportional to the film thickness and the relative thickness is expressed from 0 to 255. Because each film is supported on a flat Si_3N_4 substrate, variations in thickness correspond to the topography of the top surface of

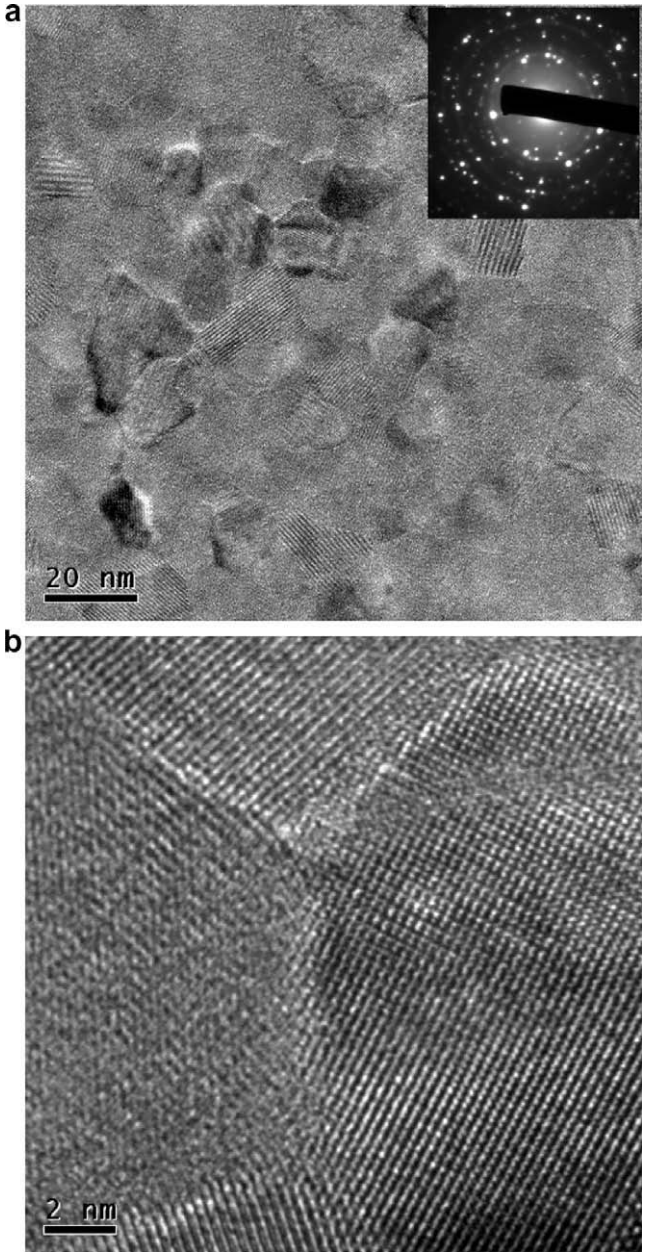

Fig. 4. Plan-view images and a corresponding diffraction pattern of a 20 nm thick ZrO_2 film that was annealed at $0.4T_m$ (922 °C) for 1 h prior to observation.

the film. As expected, we can observe the grain boundary grooves and depression at the TJs relative to the adjoining grain boundaries, in every region in the film specimen. In several cases, persistent electron interference effects are observed adjacent to the grain boundaries in the thickness images, demonstrating that the assumption of mass–thickness controlled intensity is not valid. Such cases were excluded from the analysis of TJ depression depths as described below.

The error in our thickness measurements was assessed by making measurements on a region of bare Si_3N_4 substrate which was assumed to be flat and uniform, with a thickness of 30 nm. The thickness was measured for each

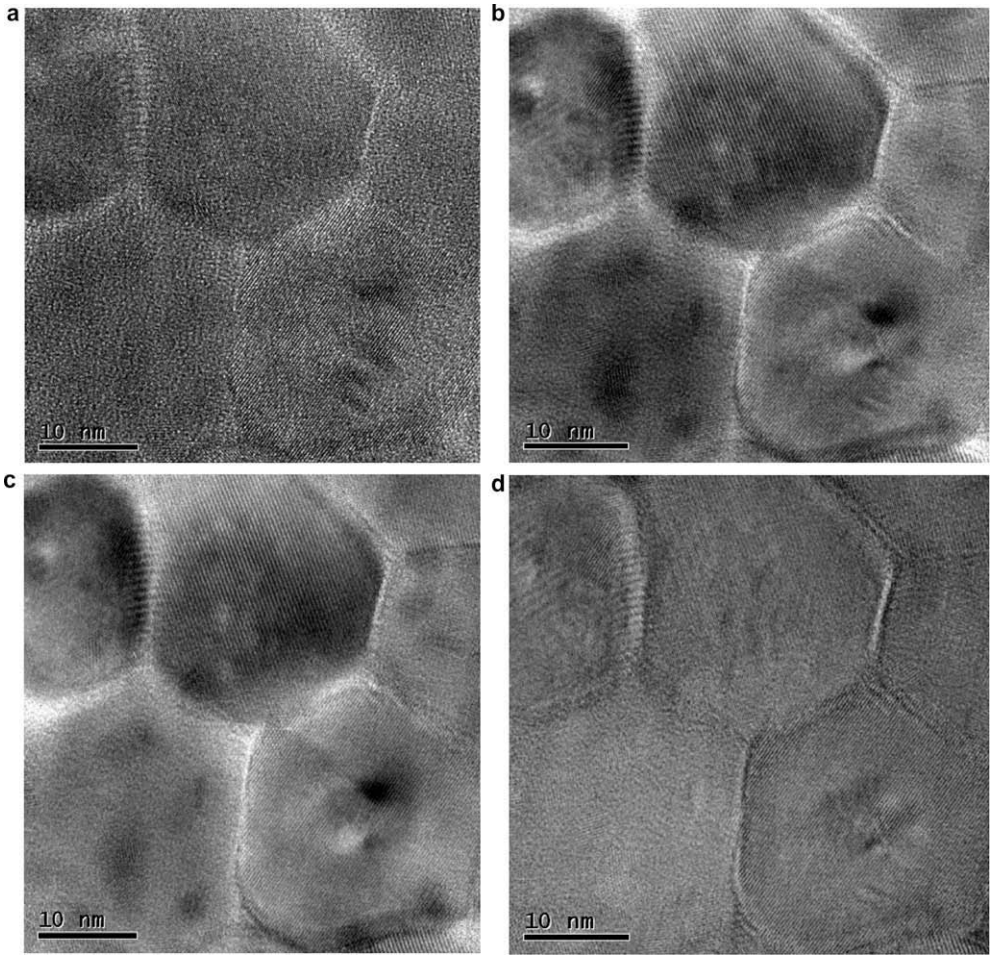

Fig. 5. EFTEM images of a ZrO_2 film illustrating the images required to form a thickness map: (a) an unfiltered multibeam image; (b) a zero-loss energy-filtered image; (c) a plasmon-loss filtered image; and (d) the thickness map derived from (b and c).

of approximately 12,000 pixels and the measurements produced a normal distribution with a standard deviation of 2.07 nm.

The grain geometry is generally similar to that of ideal hexagonal grains illustrated in Fig. 1, but the grain edge lengths are much less regular than for the ideal case. Each grain in a micrograph is assigned a unique number and individual grain boundaries and TJs are designated by the numbers assigned to the surrounding grains. For instance, grain boundary 12 denotes the boundary between grains 1 and 2, and TJ 123 denotes the TJ that defines the junction of grains 1, 2 and 3.

Fig. 6b shows the histogram of film thickness in the corresponding thickness mapping image, Fig. 6a. The estimated maximum contrast value is 153, obtained from the histogram based on the assumption that the maximum value is equal to the sum of mean value and three times standard deviation. Using this estimated maximum value, we can calculate the relative thickness. The point-by-point absolute thickness can be estimated assuming that the maximum film thickness is 20 nm and there are no pores within the film.

Film thickness variations along the grain boundary grooves were acquired from the thickness mapping images, and converted to absolute thicknesses using the information described above. Typical results are shown in Fig. 6. The expected shape of the surface along a grain boundary groove is a circular arc lying in a vertical plane if the energies of the terminating TJs energy are zero, so the thickness measurements were fitted to such a curve for each case using the method of nonlinear least-squares curve fitting. In order to exclude possible deviations near the TJs, fitting was carried out only over the central 80% of the length of each grain boundary segment, excluding the 10% of its length adjacent to each TJ.

With the noisy data from the thickness mapping images, the quality of the curve fits was typically only moderate, with R^2 values lying between 0.52 and 0.74. The fitted lines are superimposed on the detailed, point-by-point data and extrapolated to the ends of the grain boundary segments, allowing us to compare the "expected" TJ depth with the measured TJ depth.

Fig. 6c–e demonstrates a TJ depression compared to the extrapolated trace of the grain boundary groove. It can

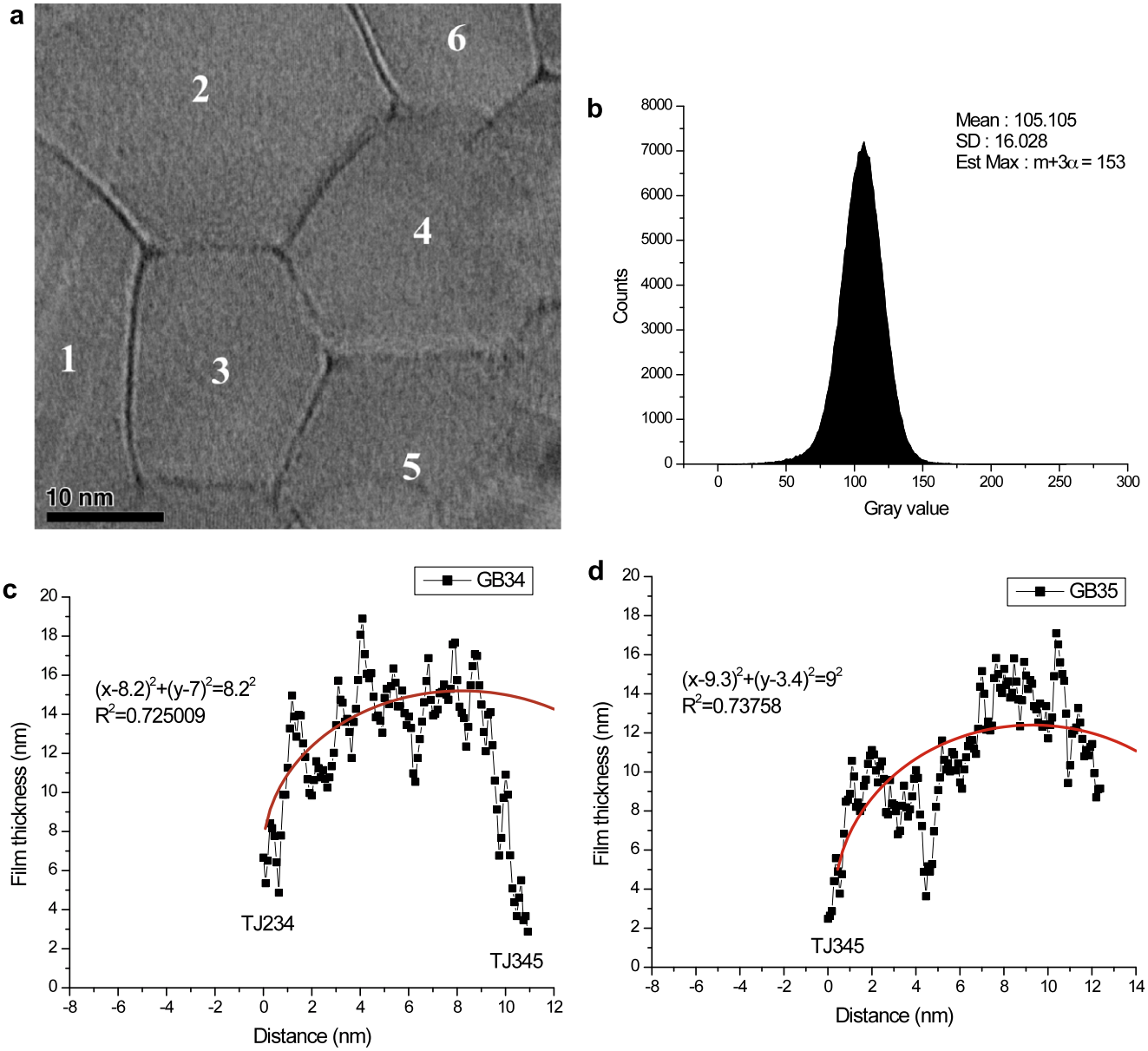

Fig. 6. Analysis of the thickness variations associated with grain boundary grooves and TJs in a ZrO_2 film: (a) is the thickness map, and (b) represents the population density of the pixels in (a) having various gray levels; (c–e) show the measured and fitted thickness variations along the grain boundary grooves that adjoin the TJ designated as 345. This TJ represents a deep pit in the film surface, and also a significant deviation from the projected grain boundary groove profile for GB34, though less distinctly for GB45 and GB35.

clearly be seen that as the distance from the center of grain boundary increases to the TJ, the film thickness decreases drastically. At TJ 345, the film thickness is only 2–3 nm, corresponding to only 1/10 of the film thickness, and the groove profiles for grain boundaries 34, 35 and 45 all depart sharply from the expected shape as they approach the TJ.

A second case of a depressed TJ is shown in Fig. 7, where significant deviations between the fitting and measured data for TJ 246 (also taken from Fig. 6a) are observed. The film thickness at this TJ was distinctly smaller than the extrapolated curve fits for each of the adjoining grain boundaries 24, 26 and 46.

The deep pits associated with junctions 345 and 246 from Fig. 6a are unusual, and our analysis of other junctions reveals much less evidence of a departure from the surface topography expected for the case of zero TJ energy, as shown in Fig. 8, which is more representative of most of our results. No significant deviation between the fitted curves and thickness data can be seen for the boundaries that define TJ 235, for example, and we observe similar behavior at most other TJs in the same specimen.

We have made detailed analyses of a total of 9 TJs and 16 grain boundaries that were connected either at one or both ends to the 9 analyzed TJs. Among these, we observed 2 deeper-than-expected cusps. The remaining 7 TJs show

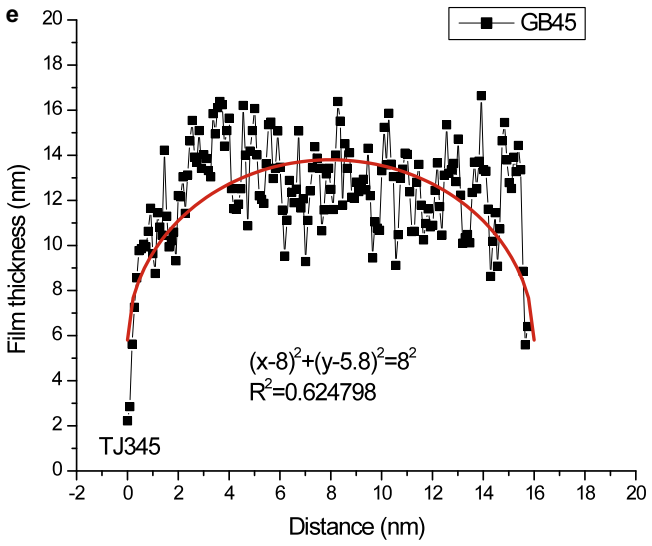

Fig. 6 (*continued*)

no significant deviation from the surface topography predicted on the basis of zero TJ energy. No cases were observed in which the TJ cusp was above the predicted depth, which would correspond to a negative TJ energy.

5. Discussion

We have applied a simple method for evaluating TJ energies of nanocrystalline ZrO_2 thin films using thickness mapping images obtained from EFTEM. Compared to the use of AFM, measurement times can be considerably reduced, though data noise is more significant in the electron microscopical technique, corresponding to the pixel-to-pixel variation of about 2 nm assessed in this work. While data noise might be reduced by increasing the image collection times, this increases the effects of specimen drift and beam damage.

The TEM technique has the advantage that deep pits can be measured without any concerns regarding steric hin-

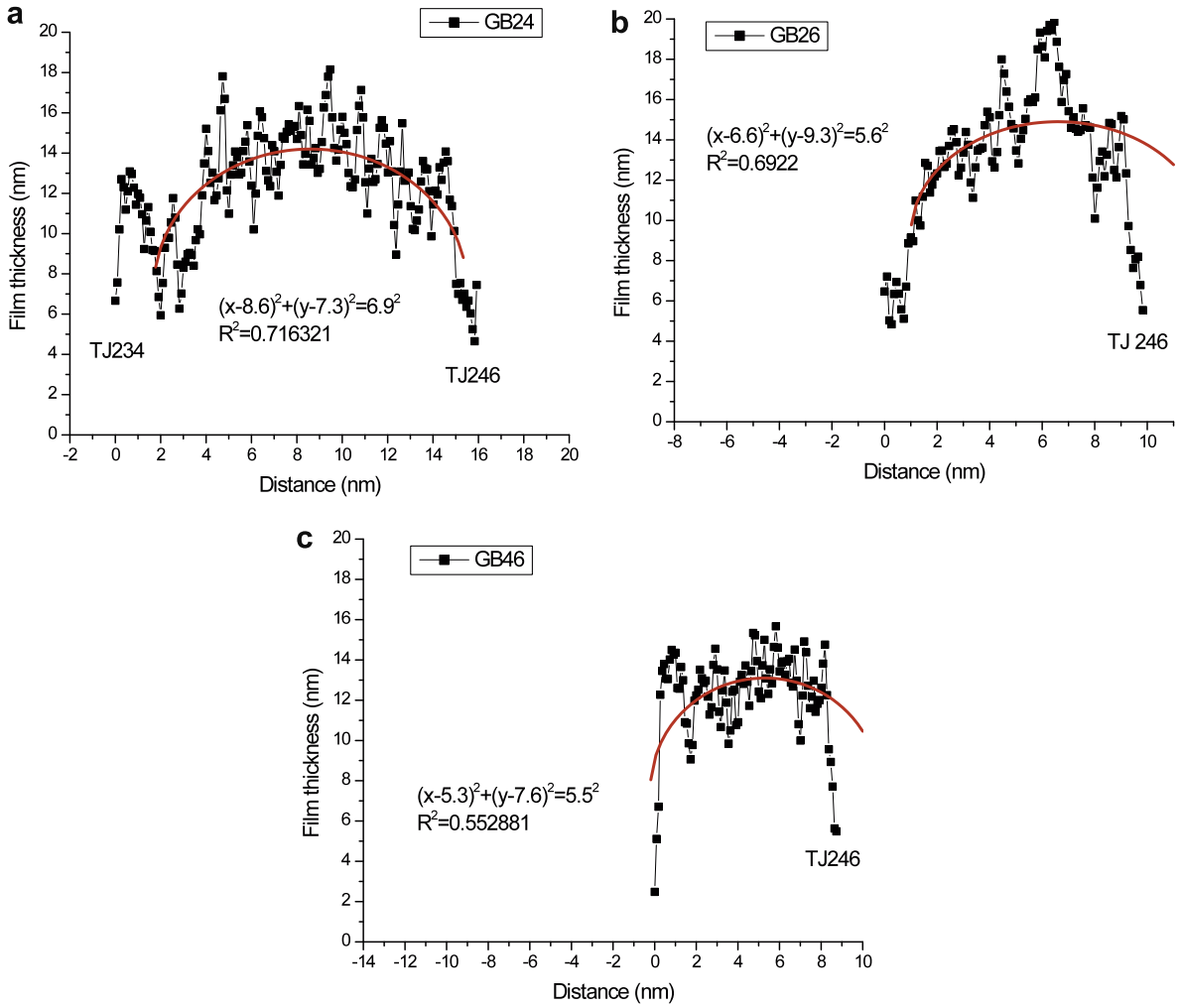

Fig. 7. Analysis of the thickness variations along the grain boundaries adjoining TJ 246 (in Fig. 6a): (a–c) measured and fitted profiles of the grain boundary grooves for GB24, GB26 and GB46, respectively. In this case, the depth of the TJ pit is not quite as great as for TJ345, but there are clear deviations from the expected grain boundary groove shapes, with each groove diving below its expected shape as it approaches the TJ, which is thus deduced to have a positive line energy.

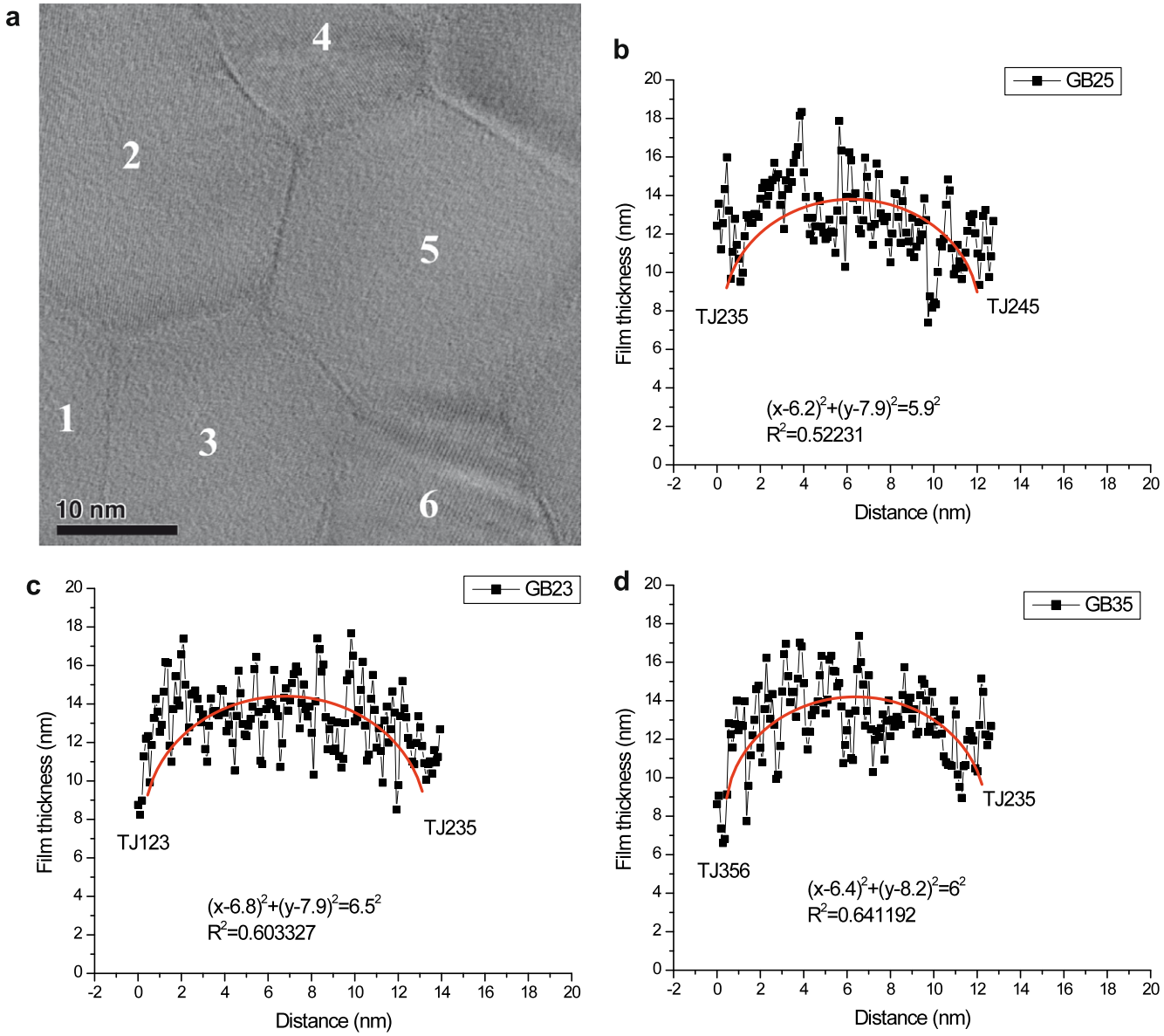

Fig. 8. Analysis of thickness variations in a case that shows no deviation from the standard behavior: (a) is a thickness map, and (b–d) are measured and fitted groove shapes for GB25, GB23 and GB35, respectively. We observe that the grain boundary grooves do not deviate significantly from the extrapolated fitted curve as they approach TJ235, implying that the standard Herring theory applies to this junction.

drance, which can prevent an AFM tip from properly reaching the bottom of a deep, narrow depression in the surface of a specimen. AFM results may fail to identify deeply cusped TJ pits, which are still accessible to the TEM.

A second potential advantage of our method, in principle, is that we can obtain the crystallographic information about the grains adjoining a TJ of interest, and deduce the misorientations of the three grain boundaries, allowing us to correlate any outlying TJ energies with the geometric characteristics of the junctions. This would allow for comparison of the deduced energies with computed values.

In this study we also tried to obtain diffraction patterns from each grain in the imaged areas using convergent-beam electron diffraction, but we were not successful because of the long times required to collect all of the information, and problems of specimen drift and radiation damage. A more effective approach would be to identify the TJs of particular interest by real-time online data analysis of the thickness data, and then collect the crystallographic data only from those junctions. This would allow the direct comparison of TJ energy observations with predictions such as those provided by Shekhar and King [21] or Nazarov et al. [8]. Automating the data analysis, however, remains quite challenging. The issues of drift and radiation damage might be ameliorated if the experiment were performed on a metallic specimen rather than an oxide, and this would be an attractive option, since TJ energy questions apply to all classes of crystalline matter, and there is at least as much concern about the structural stability of polycrystalline metal films as ceramic ones in the micro-

electronics industry. Although a metal film would not suffer from some of the challenges that we faced in this experiment, other difficulties might be anticipated, including the competition between surface equilibration and grain growth, which tends to favor larger grains and flatter surfaces for metals than for polycrystalline oxide thin films. A metal film may also undergo a number of changes over the rather extended course of our experiment, including grain growth, oxidation or the redistribution of solutes, which are not significant concerns for ceramic films like the ones we have used here. There appears to be no ideal choice of material for this experiment, but the ability to associate any particular TJ behavior with the crystallographic parameters of the junction is highly desirable.

Compared to the depth ratio measurements of Nishimura [16] and Fortier et al. [9], our method avoids the assumption of uniform hexagonal grains, and recognizes that variations in the grain edge lengths inevitably cause variations in the "reduced depth" of a TJ. Fitting the height data for each grain boundary segment to the expected circular arc also removes implicit assumptions about the energy of the "crystal–crystal–vapor" TJ that the profile represents. Even if this junction has positive energy, as argued by King [12], its shape will be a circular arc if the grain boundary TJs embody no energy.

Among the TJs for which we have unambiguous data, Fig. 7 shows no significant deviation from the grain boundary profiles expected for zero TJ energy. Fig. 8 shows an enhanced depression at the TJ, corresponding to a positive TJ energy, and no cases were found where the TJ was associated with a reduced surface depression. Our findings agree with those of Fortier et al. [9] in that all of the significant deviations at TJs may be explained by the positive TJ energy, but we cannot rule out the possibility that cases of reduced surface depth, corresponding to "negative" TJ energy, might yet be observed.

While our statistics are obviously very poor, with only 9 TJs analyzed in detail, it appears that a fraction of the order of 20% of TJs in ZrO_2 exhibit detectably elevated TJ energy.

The topographical variations associated with TJs, as observed here, may have significant impact on the performance of polycrystalline thin films in applications such as microelectronic devices or fuel cell electrolytes. Although we observed cases in which the film thickness was reduced to about 10% of its nominal value at a TJ, no case of complete perforation ("pinhole" formation) was observed.

6. Conclusions

The surface topography of polycrystals has been analyzed for the case of isotropic, homogeneous interfacial energies and zero TJ energy, to show that the depth of TJ depression is insensitive to the ratio of surface energy to grain boundary energy over a very wide range, including the values appropriate to most metals and ceramics. A critical value is found for $\gamma_g/\gamma_s \geq \sqrt{3}$, giving the condition at which TJs are replaced by hollow pipes in the absence of any excess TJ energy.

We have used EFTEM to assess the surface topography of zirconia thin films, and it is demonstrated that some TJs exhibit deep pits, indicating positive TJ energy. No cases of reduced TJ depth (which would correspond to "negative" TJ energy) have been observed. Our method has the potential to relate the crystallographic parameters of TJs to their energies.

Acknowledgments

This work was supported by the National Science Foundation, Division of Materials Research, under Grant number 0504813. Our work has benefited considerably from many enlightening and animated discussions about the topic with Prof. L. Shvindlerman.

References

[1] Palumbo G, Aust KT. Mater Sci Eng A 1989;113:139–47.
[2] Schreiber HU. Solid-State Electron 1986;29:545–9.
[3] Yin KM, King AH, Hsieh TE, Chen FR, Kai JJ, Chang L. Microsc Microanal 1997;3:417–22.
[4] Gottstein G, King AH, Shvindlerman LS. Acta Mater 2000;48:397–403.
[5] Hilden JL, King AH. Effects of triple line tension on the surface topography of polycrystals. In: Tikare V, Olevsky EA, Zavaliangos A, editors. Modeling and numerical simulation of materials behavior and evloution, vol. 731. San Francisco, CA: Materials Research Society; 2002. p. W6.7.1–6.
[6] McLean D. Grain boundaries in metals. Oxford: Oxford University Press; 1957.
[7] Schaefer HE, Wurschum R, Birringer R, Gleiter H. Phys Rev B 1988;38:9545–54.
[8] Nazarov AA, Bachurin DV, Shenderova OA, Brenner DW. Interface Sci 2003;11:417–24.
[9] Fortier P, Palumbo G, Bruce GD, Miller WA, Aust KT. Scripta Metall Mater 1991;25:177–82.
[10] Gibbs GW. Trans Connecticut Acad Arts Sci 1874:3.
[11] Srinivasan SG, Cahn JW, Jonsson H, Kalonji G. Acta Mater 1999;47:2821–9.
[12] King AH. Mater Sci Technol – Lond 2007;23:505–8.
[13] Egerton RF. Energy-loss spectroscopy in the electron microscope. New York: Plenum; 1996.
[14] Malis T, Cheng SC, Egerton RF. J Electron Microsc Tech 1988;8:193–200.
[15] Image J. <http://www.rsb.info.nih.gov/ij/index.html>. Bethesda, MD: National Institutes of Health.
[16] Nishimura G. MASc thesis, University of Toronto; 1973.
[17] Herring C. Surface tension as a motivation for sintering. In: Kingston WE, editor. The physics of powder metallurgy. New York: McGraw-Hill; 1949. p. 143–79.
[18] Hilden JL. Unpublished work. West Lafayette: Purdue University; 2002.
[19] Beck PA, Holzworth ML, Sperry PR. Trans American Inst Min Metal Eng 1949;180:163–92.
[20] Mullins WW. Acta Metall 1958;6:414–27.
[21] Shekhar S, King AH. Acta Mater 2008;56:5728–36.